Dynamic response of aluminium matrix syntactic foams subjected to high strain-rate loadings

M. Alteneiji[1*], K. Krishnan[1], Z. W. Guan[1,2,4*], W.J. Cantwell[3], Y. Zhao[4], G. Langdon[5,6]

[1] Advanced Materials Research Centre, Technology Innovation Institute, Abu Dhabi, United Arab Emirates.

[2]School of Mechanical Engineering, Chengdu University, Shiling Town, Chengdu 610106, China

[3] Department of Aerospace Engineering, Khalifa University, Abu Dhabi, United Arab Emirates.

[4] School of Engineering, University of Liverpool, Brownlow Hill, Liverpool, L69 3GH, United Kingdom.

[5]Department of Civil and Structural Engineering, University of Sheffield, Sheffield, S10 2TN, United Kingdom

[6] BISRU, Department of Mechanical Engineering, University of Cape Town, Rondebosch 7701, South Africa.

Abstract

This paper presents experimental work to characterise the dynamic behaviour of aluminium matrix syntactic foams subjected to compression, Split Hopkinson Pressure Bar and terminal ballistic impact tests as well as blast loading. Numerical models have also been developed to simulate the dynamic response of the composite foams. The effect of strain-rate on their compressive crush behaviour has been investigated, given that the rate-dependent characteristics of these materials are required for designing dynamically loaded structures. Characterisation of the behaviour of the foam under high strain-rate loadings and the identification of the underlying failure mechanisms were also undertaken to evaluate their effective mechanical performance. The results show that the aluminium syntactic foam is sensitive to strain-rate in terms of initial stiffness, peak stress and plateau stress and show a pronounced high-rate dependence at a strain rate above 1000 s^{-1}. The concrete damage plasticity model with rate-dependent features were used to simulate the dynamic behaviour of the foams, with the failure modes being captured. The model was verified and validated against the experimental results, and predictions were made for the normal and oblique ballistic impact response. Overall, the level of agreement between the numerical simulations and the experimental results is encouraging.

Keywords: metal matrix syntactic foam; blasts; impact; strain-rate; finite element.

* M. Teneiji, email: malteneiji@tii.ae, * Z.W. Guan, email: zhongwei.guan@tii.ae

1. Introduction

The resistance of engineering structures to blast and impact loads is currently of great interest within the engineering community. This is primarily due to the need for protective systems against possible terrorist attacks. The development of lightweight, strong and impact-resistant materials to manufacture special vehicles is a challenging task facing the materials community. When subjected to blast or impact loading, a structure usually undergoes large plastic deformations, possibly leading to partial or total failure. The important characteristics of such a structural response are related to: (1) the impulse generated from explosion and the shock wave transferred, and (2) the deformation mode and associated failure mechanisms, and (3) the energy absorption through plastic deformation and progressive damage [1].

A relatively new classification of materials, known as metal matrix syntactic foams (MMSF), has played an increasingly important role in the category of energy-absorbing materials [2-9]. These syntactic foams can be considered as two-phase composite materials, where the primary material is mostly a metal, and the secondary material is of a porous nature. These porous particles exhibit foam-like properties, thus making them ideal candidates for energy-absorption applications [2]. MMSF overcome some of the disadvantages of polymeric foams such as low heat resistivity, low modulus and strength. MMSF have the potential to be used as low weight structural parts in automotive industry, protective panelling in aerospace, naval, and deep-sea pipelines as well as in the packaging industry.

Aluminium alloys are the most commonly used matrix materials in metal matrix syntactic foams, due to their light weight [3-6, 10-22]. Other common matrix materials used for such applications are iron [8, 9], magnesium [23], titanium [24] and zinc [25-27]. Ceramic hollow spheres, usually made of Al_2O_3 [12, 15, 18, 28-31] or SiC [32], are used as the porous phase in such syntactic foam structures. Recently, structures known as bimodal syntactic foams are being manufactured with mixed fillers of varying sizes and materials to produce the porous structures [19, 33]. The effects of functionally graded syntactic foams under dynamic loading have also been studied and are reported to have superior properties compared to non-graded foams [34-36]. These MMSF are manufactured using a variety of novel techniques such as dispersion, infiltration, powder metallurgy and additive manufacturing methods [22]. The pressure infiltration technique is by far the most employed process for manufacturing

MMSF as it can incorporate a large range of reinforcement volumes compared to other methods [37, 38].

Metal matrix syntactic foams have been tested under dynamic compressive loading by a number of workers [3-5, 7, 8, 14, 23, 27, 32, 34, 36, 39-45]. It was observed that at high strain-rates, aluminium matrix syntactic foams experience higher plateau stress and peak stress values relative to those measured through quasi-static tests [36, 39, 45]. This indicates that the dynamic energy absorption capability of the aluminium foam is higher than the quasi-static value [4, 46]. Balch and Dunand [6] reported that the rate sensitivity of the aluminium matrix induces a rate-sensitivity in the aluminium syntactic foam. They found that the dynamic compressive strength of the aluminium syntactic foam was about 30–45 % higher than that of its quasi-static counterpart. In contrast, Luong et al. [32] reported that A356/SiC syntactic foam is insensitive to strain-rate. However, micro-inertia effects influence the rate-sensitivity of syntactic foams [6]. In addition, Goel et al. [40] inferred that both the size of the ceramic micro-spheres, as well as the fabrication method that was used, have an effect on the rate-sensitivity of a syntactic foam. Wang et. al. [45] studied the impact resistance of Aluminium syntactic foams, highlighting the effect of bio-inspired nacre like structure to mitigate damage propagation under impact loading. Aluminium foam has also been investigated under blast loading using a ballistic pendulum [1]. Radford et al. [47] studied the effect of the density of an aluminium foam core and the thickness of the cover plate on the blast response of sacrificial cladding panels.

To date, detailed information on the dynamic response of aluminium matrix syntactic foams subjected to high strain-rate loading is limited. The advantages of using MMSF structures as protective panel for vehicular systems under ballistic and blast loading have also been barely investigated. In response to this lack of information, this paper presents a series of experimental tests on aluminium matrix syntactic foams subjected to various forms of dynamic loading, including drop-weight impact, SHPB, ballistic impact and blast. In addition, finite element models are developed to predict the dynamic responses of aluminium matrix syntactic foams subjected to these loading conditions. Finally, the resulting numerical models are validated against the corresponding experimental results, in terms of stress-strain relationships and failure modes. In addition, oblique impact response of the foams are predicted using the validated model.

2. Experimental Procedure

In the present work, aluminium matrix syntactic foams based on ceramic spheres in the size ranges (diameter) of 25–75 μm (CM(I)), 100–250 μm (CM(II)) and 250–500 μm (CM(III)) were produced by pressure infiltration casting. The matrix was based on aluminium alloy Al7075-T. The volume fraction of the ceramic microspheres within the foam was 66 % (weighing 6 g), with aluminium matrix material representing the volume fraction of 34 % (weighing 45 g). Figure 1 shows a micrograph of the aluminium matrix syntactic foam, which indicates that some ceramic micro-spheres were fully infiltrated with molten aluminium.

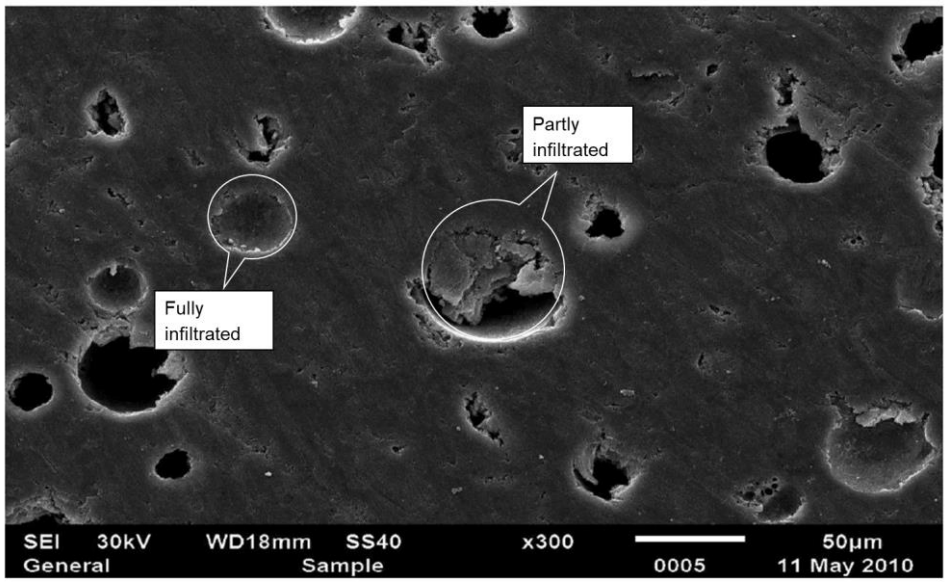

Figure 1. Micrograph of the aluminium syntactic foam showing regions where the micro-spheres are partly infiltrated with aluminium.

2.1 Compression tests

Uniaxial quasi-static compression tests were conducted on cube-shaped specimens having dimensions of approximately 20×20×20 mm^3, i.e. with a height to width ratio equal to one. The thickness of each specimen was therefore greater than seven times the size of the cells. Stress-strain curves were recorded at a crosshead displacement rate of 1 mm/min. The displacements were measured from the crosshead movement after the initial engagement of the sample with both the top and bottom platens. The strain was approximately calculated by dividing the displacement by the original sample length, whilst the stress was computed by dividing the applied load by the initial cross-sectional area.

2.2 Split Hopkinson Pressure Bar (SHPB) Tests

The SHPB apparatus employed in this study consists of two long slender bars, a striker and an output system. The specimen is positioned between the bars and loaded by a transmitted wave generated by the striker bar through the input bar. As the striker bar impacts the end of the input bar, an elastic compression pulse is generated which travels through the input bar. At the sample interface of the input bar, a portion of the pulse is transmitted to the output bar whereas the remainder is reflected. The dynamic material properties can then be found from the superposition of the incident and reflected pulses. Integration of the strain-rate in the specimen gives the corresponding strain. The stress in the specimen can be determined using Kolsky's relation [48]:

$$\sigma_s(t) = E\frac{A_0}{A}\varepsilon_t(t) \tag{1}$$

where $\sigma_s(t)$ is stress in the specimen, E is the elastic modulus of the pressure bar, A_o is the cross-sectional area of the output bar, A is the cross-sectional area of the specimen, and $\varepsilon_t(t)$ is the transmitted strain.

During Split Hopkinson Pressure Bar testing, a number of factors can affect the test accuracy [48]. These include the dispersion of the longitudinal waves, the mismatch of the impedance between the bars and the specimen and the transducer properties. However, the impedance was ensured to be matched in the SHPB test. A basic rule in selecting bar materials is to use steel bars for the harder materials (metallic ones) and aluminium bars for the softer materials (polymers, foams, etc.). Also, the end faces of the bars need to be flat and parallel to each other. Therefore, the steel bar is used in the current study. The strain in the specimen can be calculated as follows:

$$\varepsilon_s = \frac{2c_o}{L}\int \varepsilon_r(t)dt \tag{2}$$

where c_o, ε_t, ε_i, ε_r are the longitudinal wave velocity, the transmitted strain, incident strain and the reflected strain, respectively.

2.3 Ballistic Impact Tests

The ballistic tests were conducted using the firing range at Cranfield University. The length of the indoor range is 20 metres. The range is equipped with an MS instrument ballistic computer, located

in an adjacent control room. A computer is connected to sensors mounted at 6 and 10 metres down the range, which are used to measure the velocity of the projectiles. Figure 2 shows the views of the small arms experimental range and the equipment used for the ballistic impact trials. A target disc of aluminium matrix syntactic foam was fully bonded to peripheral surface of a hole in an aluminium plate, which was fixed to the stand using a panel clamp.

The labels marked 1 and 2 in Figure 2(a) are the two velocity sensors. The projectiles used in these tests were the Russian AK47 7.62 × 39 mm Kalashnikov with mild steel core [49]. The bullet consists of four main components: the projectile, the propellant, the jacket or cartridge case and the primer or igniter.

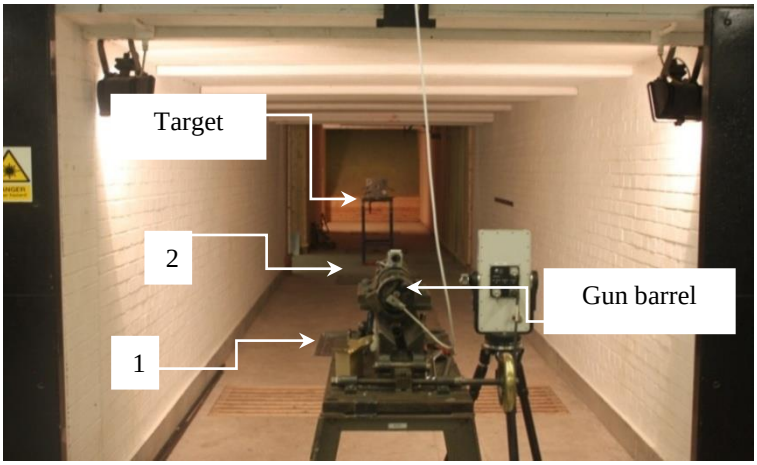

(a) Photograph of the ballistic range at Cranfield University.

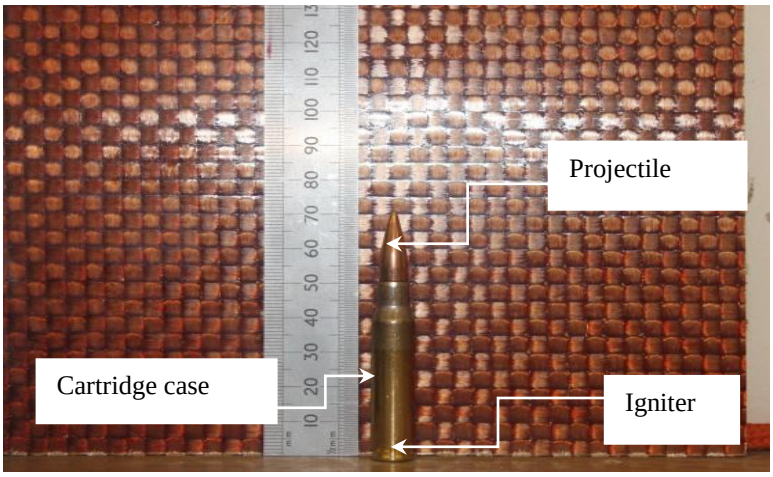

(b) The 7.62 x 39 mm (NIJ level III).

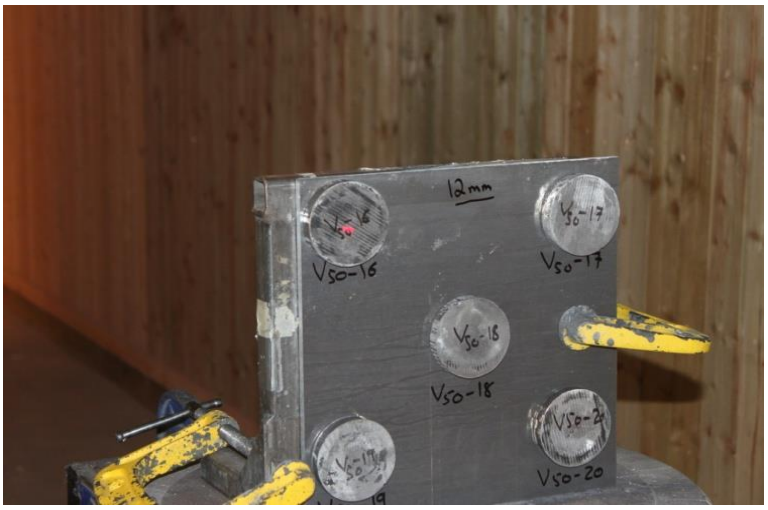

(c) Target clamped to the stand.

Figure 2. Set-up for ballistic testing

2.4 Blast Tests

Blast loads were generated by detonating 20 mm diameter disks of plastic explosive PE4 using an electrical detonator. The specimens comprised discs of an aluminium syntactic foam of varying thickness. The blast tests were carried out on samples with a diameter of 90 mm and a thickness between 3 and 20 mm**.** Here, a ballistic pendulum [50] was used to determine the impulse transferred to the specimen, as shown in Figure 3a. The explosive was attached to a polystyrene disc (13 mm thick, 90 mm diameter). PE4 consists of 12 % of lithium and 88 % of RDX grease, has a nominal density of 1600 kg/m^3, and can generate a wave velocity of 8200 m/s [51]. The blast load was directed along a 90 mm internal diameter, 180 mm long, steel tube to give a stand-off distance required and to ensure the impulse inferred from the pendulum swing was entirely directed at the panel, following [52, 53]. Steel clamps were used to provide a circular aperture and mount the specimen to the pendulum. The loading arrangement is shown in Figure 3b.

The ballistic pendulum consists of an I-beam that is suspended on 4 spring steel cables, which are attached by 4 screws that are adjustable in order to level the pendulum. Counter balancing masses are added to the end of the pendulum to ensure that each spring steel cable carries an equal load. The explosive charge generates an impulse through the centroid of the pendulum. The charge masses were 1.0, 1.5, 2.0, 2.5 and 3.0 grams with a leader of explosive fixed at 0.5 grams for the blast loading directly

onto the foam specimens (180 mm stand-off distance), For the panels with steel cover plates, the charge masses were increased to be 10, 11, 12 and 12.5 g.

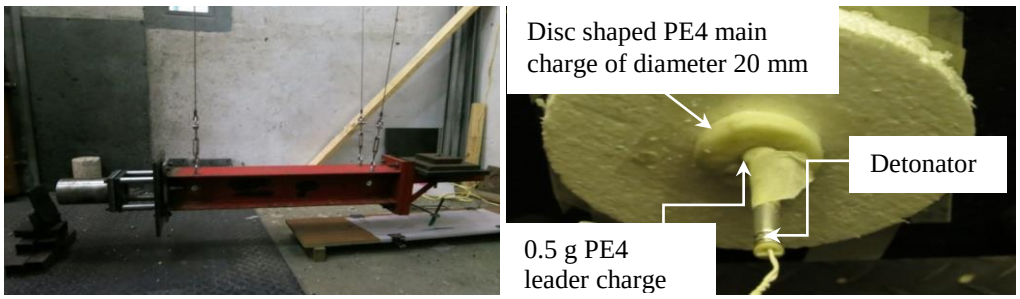

(a) the ballistic pendulum, (b) disc-shaped PE4 explosive with a 0.5 g leader attached to the detonator

Figure 3. Blast test setup

3. Finite element modelling

The commercial finite element (FE) code ABAQUS/Explicit [54] was used to model the response of the aluminium matrix syntactic foam under the different loading conditions.

3.1 Plasticity model for quasi-brittle materials

The volume fraction of the ceramic microspheres within the foam was 66 %, corresponding to a weight fraction of 88 %, which makes the deformation behaviour predominantly brittle in nature. A detailed investigation of the experimental samples reveals typical damage observed in brittle materials, such as ceramics, for instance micro-cracks and fracture. Constitutive models, such as Johnson-Holmquist (JH) or Concrete Damage Plasticity (CDP), can be candidates to be adopted to predict brittle fracture and the crack evolution observed in the experiments. However, the ability to input the stress-strain data during compressive behaviour makes the CDP constitutive model a suitable candidate to study damage in syntactic foams.

The concrete damage plasticity model provides a general capability for modelling brittle materials using concepts of isotropic damaged elasticity combined with isotropic tensile and compressive plasticity [26]. The model incorporates the two main failure mechanisms observed in brittle materials, these being tensile cracking and compressive crushing. The evolution of the yield surface is controlled by two hardening variables $\tilde{\varepsilon}_t^{pl}$ and $\tilde{\varepsilon}_c^{pl}$ linked to failure mechanisms under tension and compression

loading, respectively. The uniaxial tensile and compressive responses of a brittle material as characterised by damaged plasticity are shown in Figure. 4.

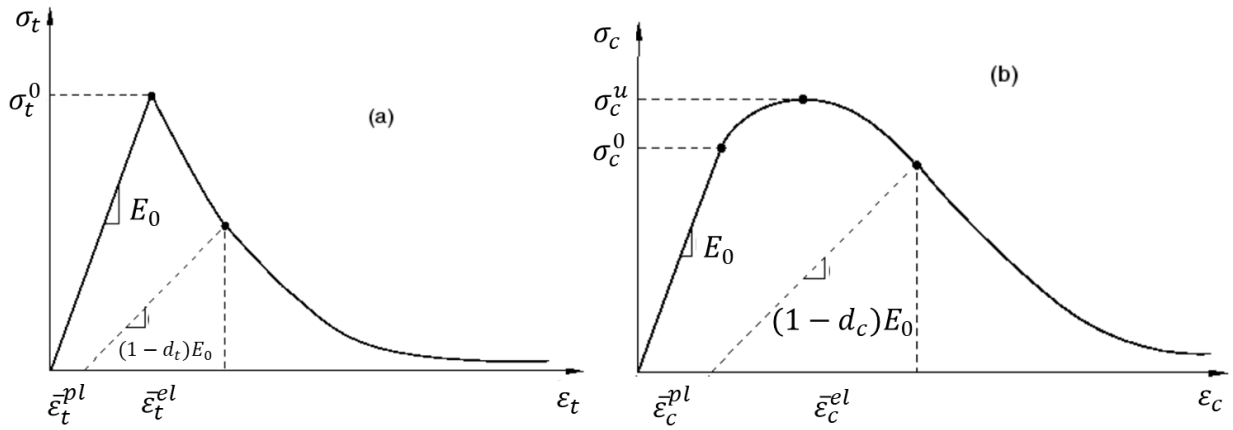

Figure 4. Uniaxial behaviour in concrete damaged plasticity model under (a) tension and (b) compression [54]

The total strain-rate $\dot{\varepsilon}$ can be decomposed into its elastic and plastic counter parts, $\dot{\varepsilon}^{el}$ and $\dot{\varepsilon}^{pl}$, i.e.

$$\dot{\varepsilon} = \dot{\varepsilon}^{el} + \dot{\varepsilon}^{pl} \tag{3}$$

The elastic damage constitutive relationship is defined as,

$$\sigma = (1-d)D_0^{el}:\left(\varepsilon - \varepsilon^{pl}\right) = D^{el}:\left(\varepsilon - \varepsilon^{pl}\right) \tag{4}$$

where D_0^{el} is the undamaged elastic stiffness of the material, d is the damage factor with the value of zero indicating undamaged material and the value of one showing fully damaged one. The concrete damage plasticity model assumes non-associated potential plastic flow. The flow potential G used in this model is the Drucker-Prager hyperbolic function:

$$G(\bar{\sigma}) = \sqrt{(e\sigma_{t0}tan\psi)^2 + \bar{q}^2} - \bar{p}tan\psi \tag{5}$$

where ψ is the dilation angle, σ_{t0} is the uniaxial tensile stress at failure, e is an eccentricity parameter and q is the equivalent stress. The material properties used in the brittle failure model were density = 2296 kg/m^3, Young's modulus = 4.00 GPa (corresponding to 66 % volume fraction of hollow ceramic microspheres) and Poisson's ratio = 0.29, dilation angle = 40^o, eccentricity = 0.1, ratio of initial equibiaxial compressive yield stress to initial uniaxial compressive yield stress is 1.16. These material

constants were calibrated within the specified range values using the quasi-static compression test data[54]. The compressive stress-strain data were obtained from experiments as shown in Table 1. Concrete failure criterion is used to define the material failure based on tensile cracking strain. When it exceeds a critical value, element deletion will be triggered. Special care needs to be taken, while inputting the post damage strain values as Abaqus will issue error warning if the calculated plastic strain values are negative or decreasing with increasing cracking strain.

Table 1. Concrete compression and tension data for the brittle failure model

Compressive Behaviour		Tensile Behaviour		
Yield Stress (MPa)	Inelastic Strain	Yield Stress (MPa)	Cracking Strain	Damage Parameter
184.79	0	75	0	0
185	0.012717	70	0.00156	0.0010
186	0.061272	62	0.00257	0.0018
186.2	0.067052	56	0.00357	0.0025
186.4	0.077457	40	0.00453	0.0035
186.6	0.116763	44	0.00549	0.0050
191.977	0.216185	38	0.00645	0.0060
195.398	0.261272	32	0.00741	0.0070
196.6	0.285549	26	0.00837	0.0085
204.357	0.322543	20	0.00933	0.1000
222.092	0.378035	14	0.01029	0.2000
191.977	0.216185	8	0.01125	0.3000
195.398	0.261272	2	0.017	0.6500
260.725	0.440462	0	0.04	0.9000
307.025	0.493642			
363.203	0.542197			
409.452	0.576879			
457.883	0.60578			
380	0.63			
320	0.65			
260	0.67			
180	0.69			
90	0.71			
40	0.72			
10	0.73			

3.2 Finite element model setup

3.2.1 Modelling of the compressive behaviour of the syntactic foam

The setup for the compression test used for the simulations is shown in Figure 5. A 20×20×20 mm^3 cubic model was created, similar to the test sample. Very fine 8-noded hexahedral elements (C3D8R), with reduced integration and an element size of 0.2 mm, were used to capture the crack formation and damage evolution within the sample. The refined mesh, though computationally expensive, helps in

capturing crack propagation due to tensile failure without leading to any instabilities. The stress-strain values for the syntactic foam CM(I) were obtained from the compression test. Displacement was applied to the top rigid plate while the bottom rigid plate was fully constrained.

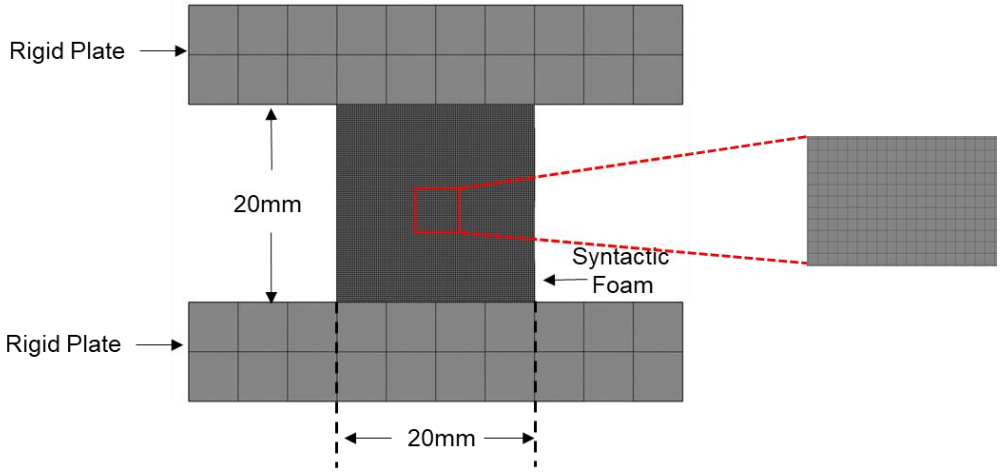

Figure 5. Finite element model for the compression test

3.2.2 *Modelling ballistic impact*

Simulations of the ballistic tests were carried out to identify the minimum thickness of foam required to prevent perforation of a bullet. Boundary conditions similar to the experiments were used in the model. The mesh density in the central area of the sample was higher than that in the outer regions. The failed elements were removed during the penetration process. Figure 6(a) shows the finite element setup for the ballistic impact simulations. The outer surface of the sample was fully constrained. An initial velocity was applied to the projectile, equal to the impact velocity measured in the test. The residual velocity and depth of penetration were predicted using the model. The detailed bullet model is shown in Figure 6(b). The steel core, copper jacket and lead filler are modelled using Johnson-Cook constitutive model [55] and the parameters are summarised in Table 2. Effective plastic strain is used as the damage criterion with element deletion enabled in order to avoid excessive distortion.

Table 2. Johnson-Cook material properties for projectile components[56]

	A (MPa)	B (MPa)	C	n	m
Steel Core	234.4	413.8	0.0033	0.25	1.03
Copper Jacket	448.2	303.4	0.003	0.15	1.00
Lead Filler	10.30	41.3	0.001	0.21	1.03

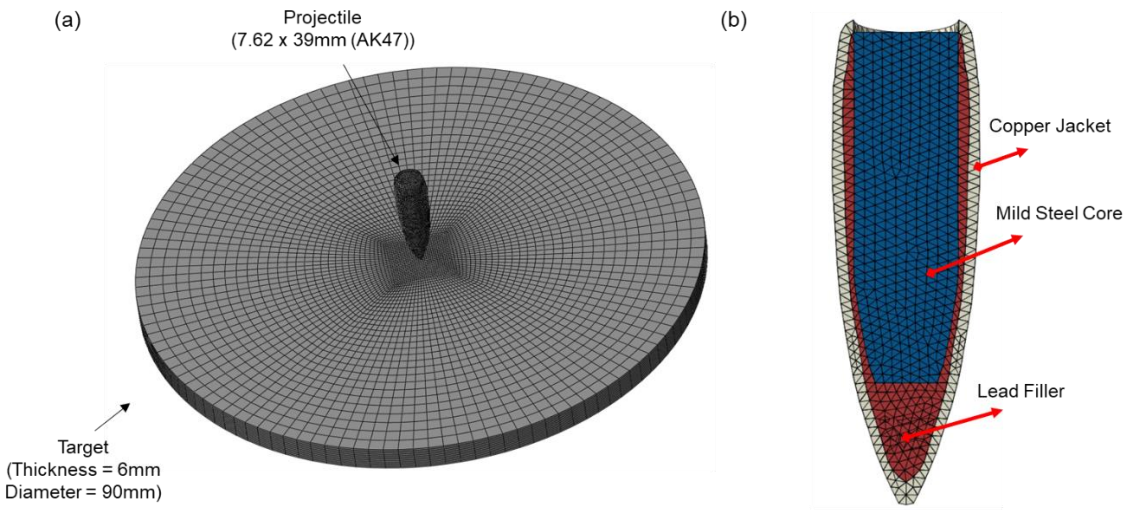

Figure 6. Finite element model setup for terminal ballistic impact (a) FE mesh for the setup (b) Projectile mesh and components

3.2.3 *Modelling blast behaviour*

The numerical model was developed to simulate the blast response of the foam subjected to such the extreme loading condition. The mesh generation, shock pressure distribution and boundary conditions are shown in Figure 7. The model is subdivided into two separate zones over which different impulse pressures were applied. The outermost circular ring is clamped to simulate the boundary conditions used in the blast experiments. The pressure distributions for the two zones were proposed by the authors [57] and were adopted here.

$$P_{total} = P_1 + P_2 = \frac{0.85 I_m}{2A_1 t} + \frac{0.15 I_m}{2A_2 t} \quad (6)$$

where I_m is the impulse obtained from experimental measurements, $A_1 + A_2$ is the total pressurised area and t is the blast time in microseconds. A highly refined mesh ($0.1 \times 0.1 \times 0.1mm$) is used in the zone A_1 in order to capture the damage evolution of cracks during blast loading (Fig. 7). The area close to the clamped boundary was also locally refined to capture the damage observed in the adjacent regions, due to the high stress concentration there.

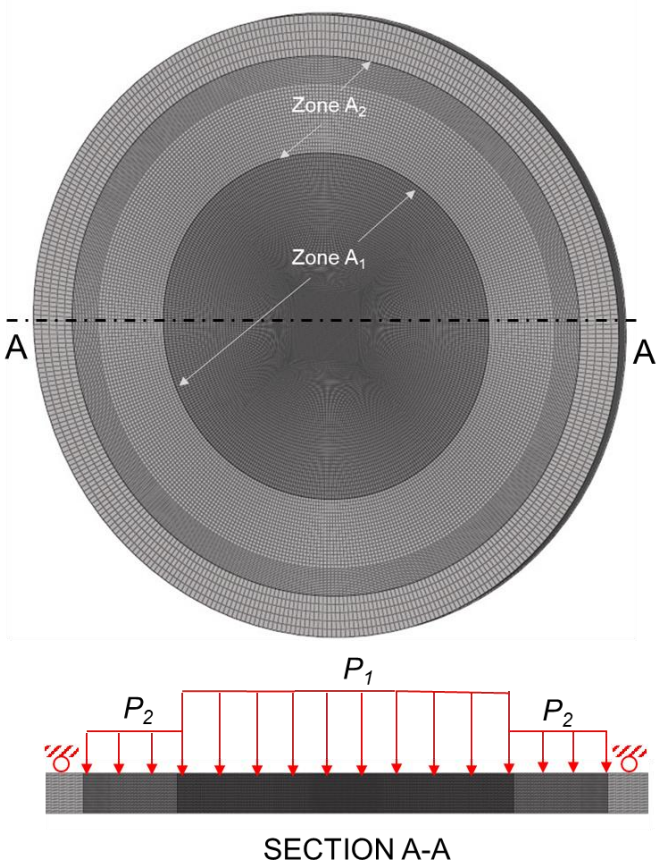

Figure 7. The finite element model setup showing the mesh generation, shock pressure zones and boundary conditions.

4. Results and Discussion

4.1 Experimental results

4.1.1 Compression test results

The compressive stress-strain curves of the different syntactic foams for the quasi-static and dynamic compression tests are shown in Figure 8. The stress values are normalized with respect to the plastic collapse stress to ensure consistency between the different material densities. There are three typical phases observed during the compression response of cellular solids. Initially, a linear elastic phase is observed, where the strain is less than 3 % and the stress–strain relationship follows Hooke's law. The slope of the first part is defined as the Young's modulus. This is followed by a section where the peak stress is reached, plastic deformation of the matrix starts and the load transfer between the matrix and ceramic micro-spheres reaches its maximum. This is where the compressive strength is

measured. Next, there is a small reduction in stress, due to the reduced load-bearing capacity caused by crushing of the ceramic micro-spheres and global instability. The second phase occurs between strains of 10 % and 43 %, characterised by a relatively constant plateau stress, where the micro-porosity in the ceramic micro-spheres densifies through crushing. Energy absorption is significant in this region, as the stress remains constant with increasing strain. The final phase is associated with densification, where the stress increases to a high value very quickly, while the strain increases slowly. The densification strain is located at the intersection between the tangents of the densification phase and the plateau phase. The mechanical properties of the syntactic foams are listed in Table 3, which are based on three repeated test results of each specimen.

Table 3. Average mechanical properties of aluminium matrix syntactic foams

ID	Density (kg/m^3)	Plastic Collapse Stress, σ_{pl} (MPa)	Compressive Modulus (GPa)	Steady State Stress, σ_{ss} (MPa)	Densification strain, ε_D (%)
CM(I)	2388	179	3.22	175	36
CM(II)	2321	167	2.83	150	41
CM(III)	2250	160	2.45	148	43
CM(IV)	1790	130	2.40	128	43
CM (V)	1680	101	2.25	78	44
CM(VI)	1585	75	2.10	65	50

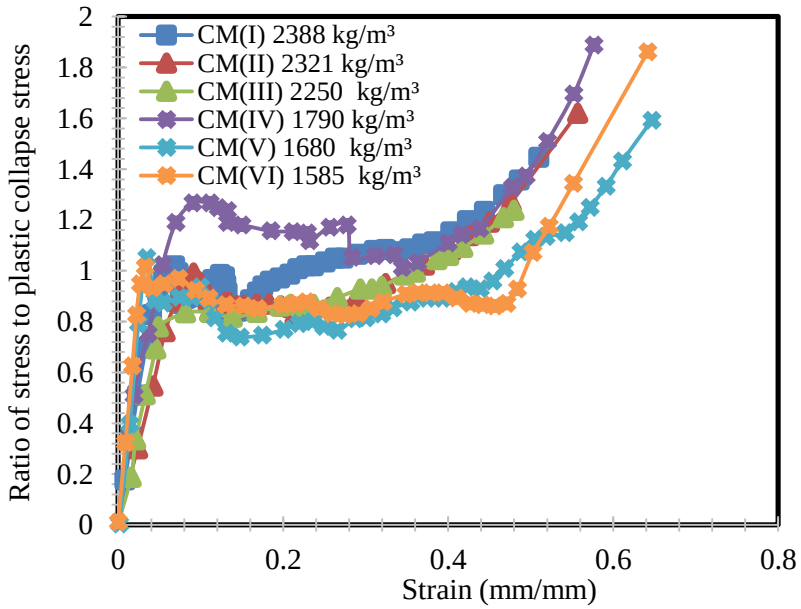

Figure 8. Quasi-static stress–strain curves of the compression tests on the aluminium matrix syntactic foams

4.1.2 Impact response from Split Hopkinson Pressure Bar (SHPB) tests

The dynamic properties of the aluminium syntactic foams are listed in Table 4. The failure modes observed in the aluminium syntactic foam at high strain-rates were associated with compressive failure, rather than shear failure. It is possible that the high strain-rate during the test hindered the formation of shear band. A strain-rate sensitivity parameter ($\sum$) was used to evaluate the effect of strain-rate on the material under dynamic loading, which can be calculated using the following equation [9]:

$$\sum = \frac{\sigma_d - \sigma_q}{\sigma^*} \left[\frac{1}{\ln \frac{\dot{\varepsilon}_d}{\dot{\varepsilon}_q}} \right] \quad (8)$$

where σ is the flow stress, σ^* is the static stress at 5% strain at a strain-rate of 10^{-3} s^{-1} for foam materials, $\dot{\varepsilon}$ is the strain-rate and *d* and *q* are subscripts that refer to dynamic and quasi-static testing, respectively. The peak stress reached in compression is used to calculate the sensitivity parameter, although these peak stresses appear at slightly different strains. The strain-rate sensitivity parameters of various aluminium alloys are varied between 0.006 and 0.06. Table 4 shows that the sensitivity parameter of the aluminium syntactic foams lies between 0.018–0.204, which indicates that this type of the aluminium syntactic foam is sensitive to strain-rate. Figure 9(a) shows the strain pulses obtained from the incident and transmitted bars used to compute stress, strain and strain rate. The combined reflected and transmitted strain pulses are plotted along with the incident pulse, as shown in Figure 9(b), to identify any potential losses in the specimen while testing. The close match ensures that the losses are not significant during the tests.

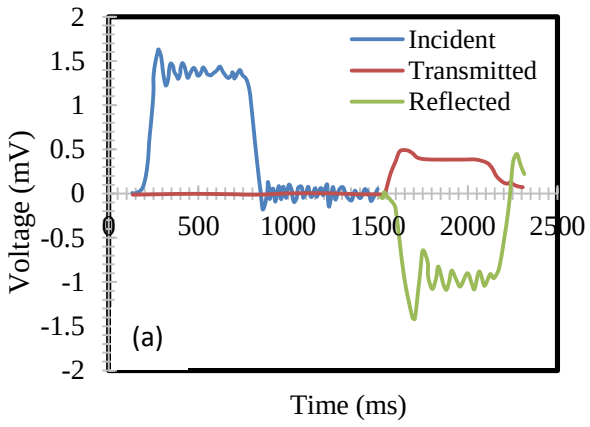

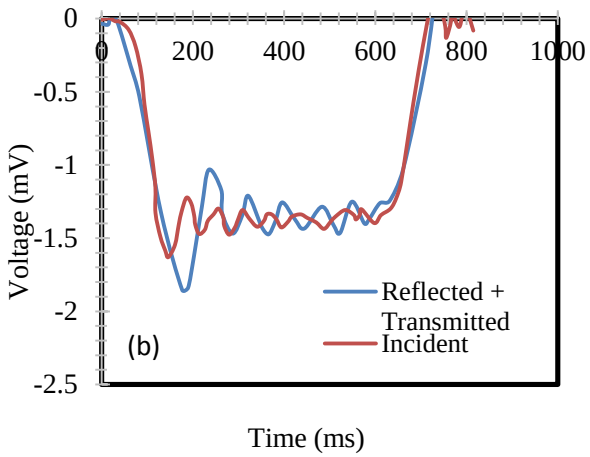

Figure 9. Split Hopkinson Pressure bar test results for a representative Aluminium syntactic foam showing (a) strain signals from incident and transmitter bars (b) comparing strain signals to analyse losses in the specimen

Table 4 Average high velocity impact properties of the aluminium matrix syntactic foams (CM (I), CM (II) and CM (III).

ID	Young's Modulus (GPa)	Dynamic compressive strength (MPa)	Dynamic strain rate (1/s)	Relative density, (ρ/ρ_s)	Relative yield strength, (σ/σ_s)	Relative Young's modulus, (E/Es)	Sensitivity parameter $\sum$
$CM(I)_1$	14.22	601.4	1578	0.891	0.752	0.151	0.204
$CM(I)_2$	13.95	574.9	1547	0.890	0.719	0.148	0.192
$CM(II)_1$	13.16	487.9	1517	0.889	0.609	0.139	0.151
$CM(II)_2$	12.87	461.0	1273	0.880	0.922	0.184	0.140
$CM\ (III)_1$	11.93	265.0	1263	0.797	0.650	0.099	0.043
$CM(III)_2$	9.04	203.0	882	0.755	0.490	0.057	0.018

* E_S, σ_s and ρ_s of aluminium Al 7075-T6 are 94.4 GPa, 646 MPa and 2810 kg/m^3, respectively [20].
*$_{1,2}$ refer to the same type of material at different strain rates.

Figure 10 shows the dynamic compressive stress–strain curves for materials CM (I), CM (II) and CM (III). The stress values are normalized with respect to the dynamic compressive strength to ensure consistency between the different material densities. The results highlight the rate-sensitivity of the foams. For example, the peak stress for $CM\ (III)_2$ increased from 203 MPa at 882 s^{-1} to 601 MPa at 1578 s^{-1} $CM\ (I)_1$. The peak stress is shifted to lower strains at higher strain-rates, as are the fracture strains, primarily due to the strain-rate sensitivity of the foam matrices (change of foam densities also plays some role). It was found that those syntactic foams with a higher percentage of metal matrix were more rate-sensitive. The results presented in Figure 11 show the influence of strain-rate on specific energy absorption, the plateau stress and the peak stress, respectively. The results confirm the dependency of the properties of the syntactic foam on strain-rate. An increase in the strain-rate leads to

an increase in the specific energy absorption, peak stress and plateau stress. In addition, the peak stress appears to be more sensitive to strain-rate than the plateau stress, which is likely due to the prolonged plateau stage. However, the strain-rate dependence is not significant until values of 1000 s^{-1} and above, where both the plateau and the peak stresses exhibit a strong rate-dependence (Figure 11(b)).

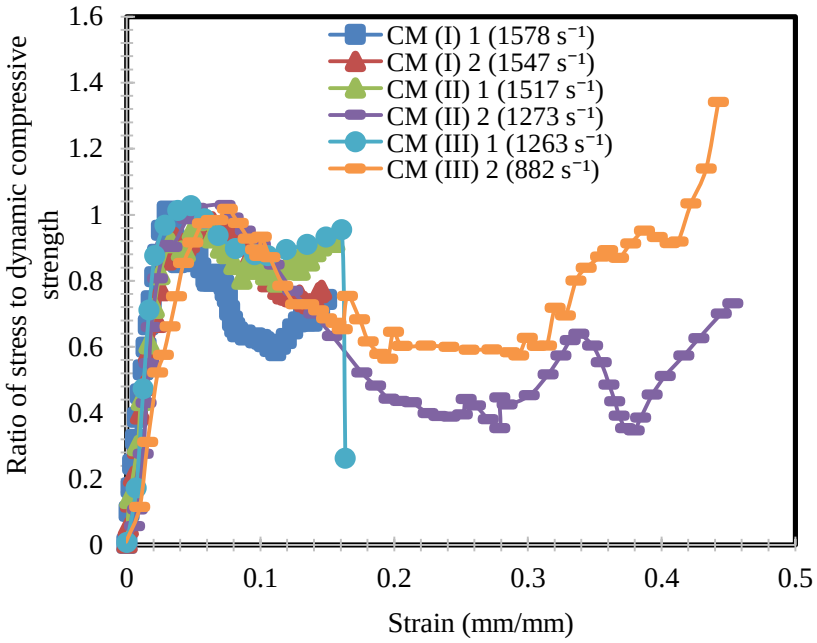

Figure 10. Compressive stress–strain curves for the aluminium matrix syntactic foam at high strain-rates

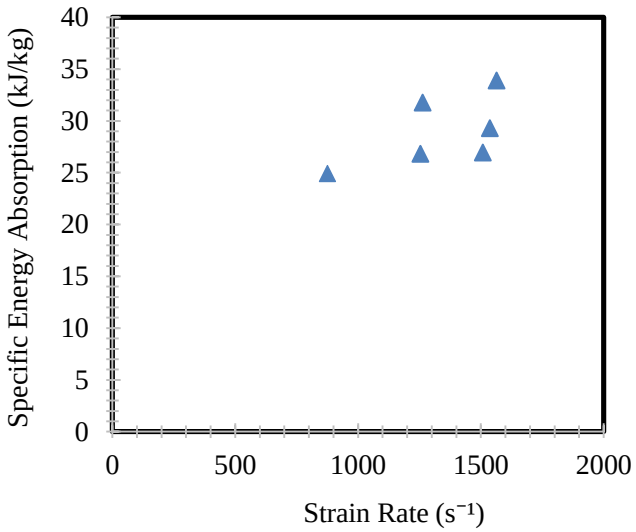

(a)

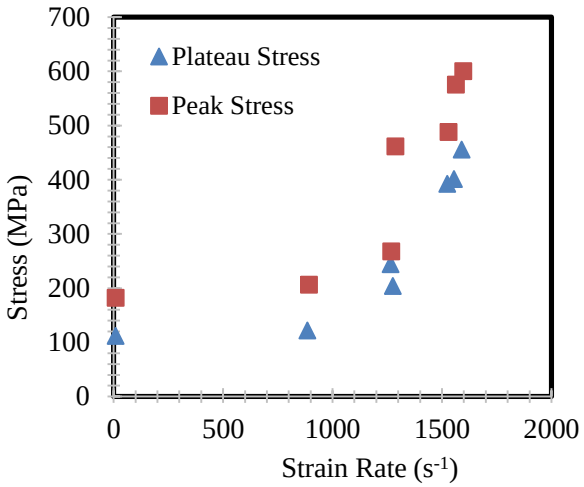

(b)

Figure 11. Strain-rate dependence of CM (I) foams (a) The variation of specific energy absorption with strain-rate (b) the variation of plateau and peak stress with strain-rate.

4.1.3 Ballistic impact behaviour

The ballistic response of different thicknesses of aluminium matrix syntactic foams was investigated using ballistic impact tests. A summary of the results from the ballistic tests is shown in Tables 5 and 6. The penetration resistance of foam CM (I) follows a linear relationship with velocity, which can be expressed as

$$DOP_{Al7075\text{-}T6\ (75\ \mu m)} = 0.5627+0.4187\ v_s \quad (9)$$

where $DOP_{Al7075\text{-}T6\ (75\ \mu m)}$ is the depth of penetration (DOP) into the foam and v_s is the impact velocity.

Table 5. Average properties and DOP for the aluminium matrix syntactic foam subjected to impact velocities up to 20 m/s.

ID	Thickness (mm)	Impact velocity (m/s)	DOP (mm)	Areal density (kg/m^2)
G1	13.2	20	8.94	18.35
G2	14	17	7.60	19.46
G3	15	14	6.50	20.85
G4	15.6	11	5.24	21.68
G5	15.6	8	3.27	21.68

Table 6. Average terminal ballistic properties of the aluminium matrix syntactic foam with same density but different thickness.

ID	Thickness of the sample (mm)	Impact velocity (m/s)	Residual velocity (m/s)
T1	6	812	740
T2	6	815	742
T3	6	845	760
T4	8	850	830
T5	8	750	727

T6	8	650	625
T7	10	550	520
T8	10	450	415
T9	10	350	310
T10	12	250	203
T11	12	150	81
T12	12	120	33

357

358 The penetration of a target by a projectile depends on the material properties, impact velocity,
359 projectile shape and target position. In addition, the prediction of target and projectile failure is required
360 in order to design a target with the minimum areal density to defeat the projectile. The parameters that
361 control perforation include the thickness of the target, the radius of the projectile and the impact velocity.
362 If the ratio of the target thickness to the radius of the projectile is greater than one, the target plate is
363 considered to be thick, whereas if the ratio is less than one, it is considered to be thin.

364 *4.1.4 Blast response*

365 A summary of the blast tests is given in Table 7, detailing the mass of explosives used for each
366 test, the impulse measured and the permanent resulting displacement. The results show that the measured
367 impulses lie between 3.09 Ns and 6.12 Ns. These results are lower than those reported by Teeling-Smith
368 and Nurick [58] for steel, due to the longer stand off distance employed in the experiments. Many of
369 samples fractured or exhibited small permanent displacements, reflecting the extremely brittle nature of
370 aluminium syntactic foam materials. The foam failed by radially cracking in several locations. This is
371 discussed more fully in relation to the finite element modelling results in Section 4.2.3. The results also
372 indicate that the charge mass increased the damage on the target, as expected.

373 Table 7. Summary of the blast tests (the stand-off distance was 180 mm).
374

ID	Sample thickness (mm)	Mass of PE4 (g)	Impulse (Ns)	Mid-point deflection (mm)
B1	3.07	1.5	3.82	*
B2	5.8	1.5	3.36	*
B3	9.12	1.5	3.09	0.45
B4	9.18	2.0	4.50	*
B5	10.0	1.0	4.20	0.50
B6	10.2	2.0	4.30	0.35
B7	10.5	2.0	4.32	*
B8	12.5	2.0	3.72	0.48
B9	12.8	2.5	5.4	*
B10	14.0	2.5	4.82	0.50
B11	16.0	2.5	4.79	0.45

B12	20.0	3.0	6.12	0.60

* Sample completely failed

4.2 Finite element modelling results

The concrete damage plasticity (CDP) material model is mostly used to study the compressive behaviour of concrete and other reinforced brittle materials. The implementation of the CDP model to study syntactic foams needs to be justified through a series of verification and validation simulations in order to use it as a predictive tool for further studies. The verification study is conducted by comparing the compressive test results obtained from the finite element models with the experimental stress-strain curves. The finite element model is then verified using ballistic test results from tests on 6 mm thick syntactic foam sample as well as the blast response of a 10 mm thick foam. The validated model is then used to predict the impact response of different thicknesses of syntactic foam subjected to normal and oblique impacts.

4.2.1 Modelling quasi-static compression behaviour of the syntactic foam

The comparison between the finite element results and the experimental compression stress-strain curve is shown in Figure 12. The FE model is capable of capturing the predominant features of the compressive behaviour, such as the plastic collapse stress, the compressive modulus as well as the steady state stress. Furthermore, the contour plots for tensile damage, as shown in Figure 13, show a good degree of correlation with the damage observed in the tested sample. The cracking occurs along a characteristic shear plane at 45^0 to the loading direction, which is consistent with the damage observed in metal matrix syntactic foams subjected to compression [59, 60]. Comparisons of the experimental and predicted compressive stress-strain curves, as well as the failure mode can be used to verify the numerical model as well as the input parameters. The plateau and peak stress values for the quasi-static stress-strain data can be scaled for testing at strain-rates related to dynamic loading using the strain-rate dependency shown in Figure 11(b).

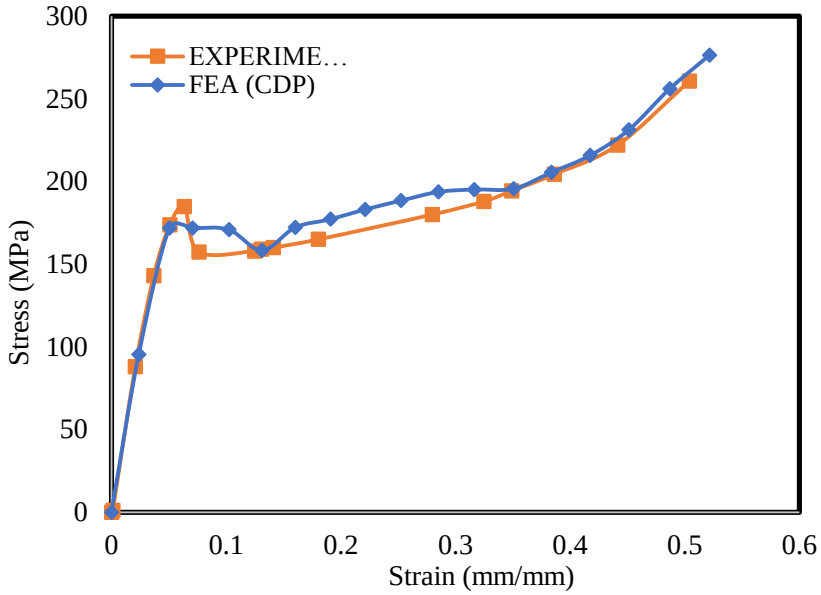

Figure 12. Verification of the FE model using the compression test experimental data

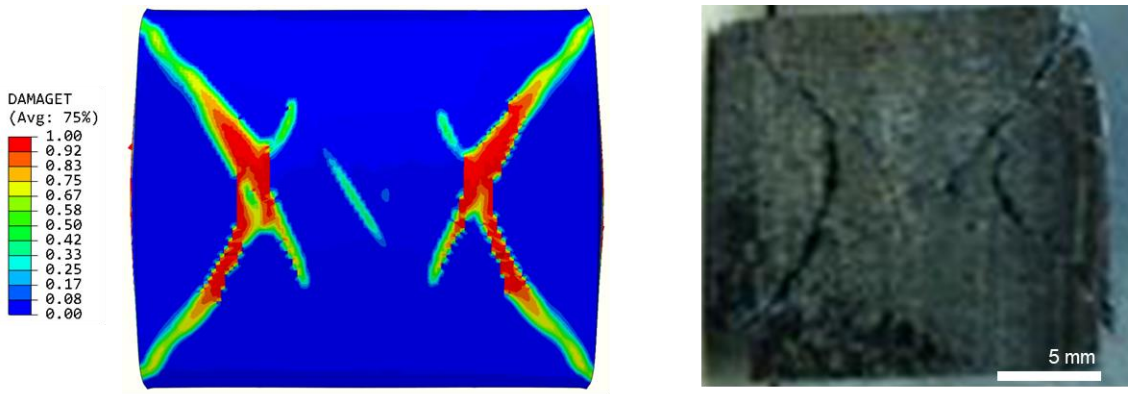

Figure 13. Crack propagation during the compression test (a) FE results showing tensile damage contour (b) Experimentally failed sample.

4.2.2 Modelling the ballistic impact response of the syntactic foam

The finite element models developed were validated against the ballistic impact and blast test results. The objective was to compare the results obtained from the finite element simulations with the experimental data without changing any of the material parameters. The syntactic foam samples with a thickness of 6 mm, were impacted at velocities of 800, 750 and 700 m/s and the corresponding residual velocities were predicted using the model. The FE simulations are compared with the experimental results in Figure 14. The predicted damage modes of the foam as well as the projectile exiting the panel are shown in Figure 14(b). As there are only two measured residual velocities, three predicted residual

velocities are obtained using the validated FE model. The method of least squares using the Lambert-Jonas equation (Eqn 10) [61] is used to apply a curve fit to the FE results, as shown by a solid line in Fig 14(a). The experimental results are then superimposed on the fitted curve generated from the simulations, which indicates reasonable correlation.

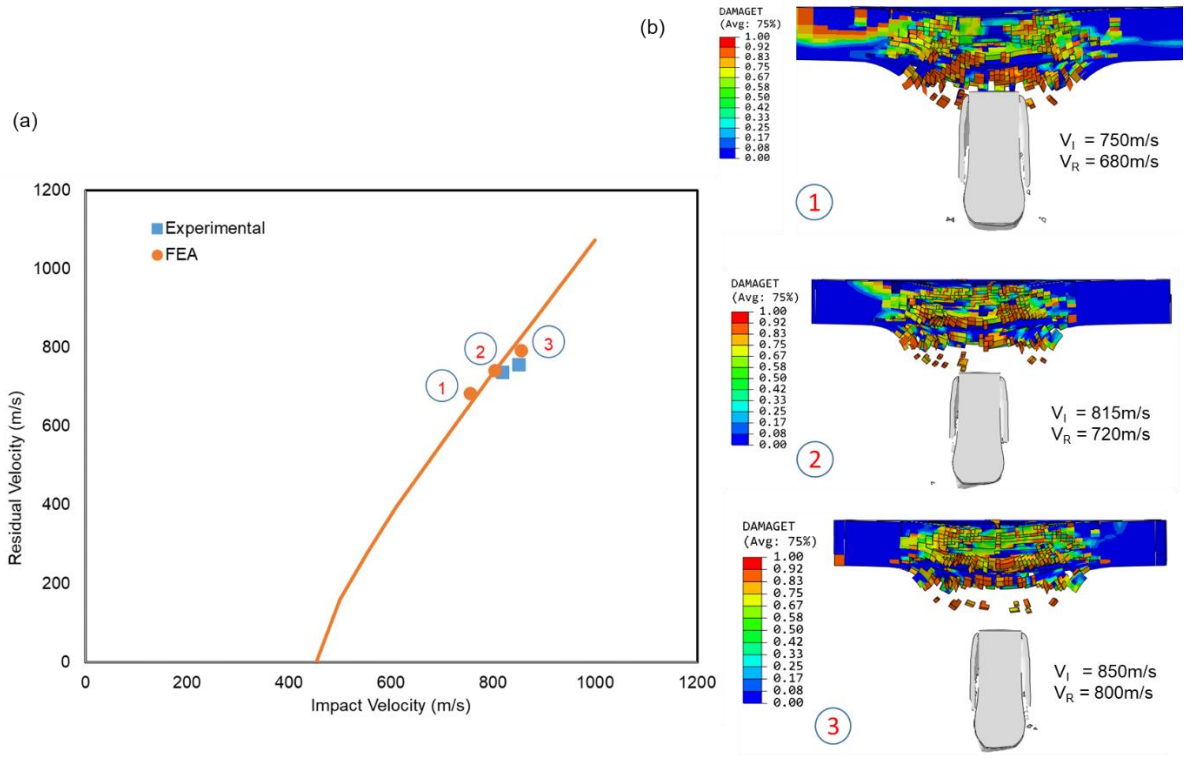

Figure 14. Validation of the FE model using ballistic limit tests on 6 mm thick syntactic foam samples: (a) residual velocity, (b) the simulated failure modes (V_I = impact velocity, V_R = residual velocity).

4.2.3 Modelling blast response

The simulations for blast tests were performed for the syntactic foams with two different thicknesses in order to predict different damage patterns observed during experiments. The validation was carried out on the damage profiles on the front and back face of the foam panels. Firstly, a thin sample (thickness = 3 mm) subjected to an impulse of 2 Ns was simulated to validate the model for the target experienced a complete failure. The front face and side views of the failed foam panel after the blast simulation are shown in Figure 15. The thin target exhibits a complete failure in the central high-pressure zone as well as the area around the clamped boundary. The failed target is compared with the corresponding experimentally failed sample in Figure 16. The FE simulations shows good correlation with respect to the size of the crater and the radial cracks that are evident in the test sample. The

simulations show more uniform damage compared to the tests due to the uniformly applied boundary conditions and loads and homogenous modelling of the syntactic foams.

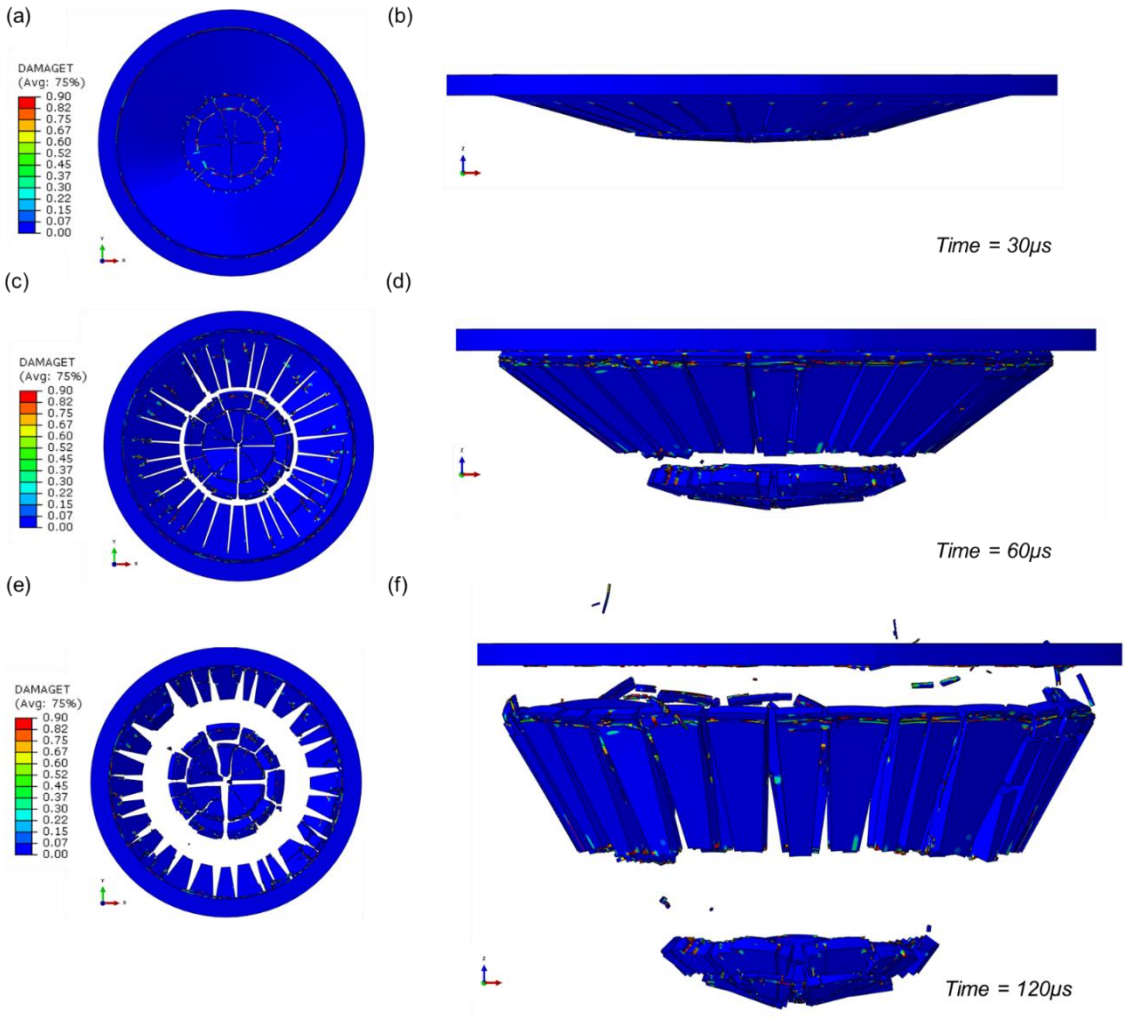

Figure 15. Front face and side views of the damage profile of a 3 mm thick syntactic foam subjected to an impulse of 2 Ns detonated at a stand-off distance of 180mm at different time steps.

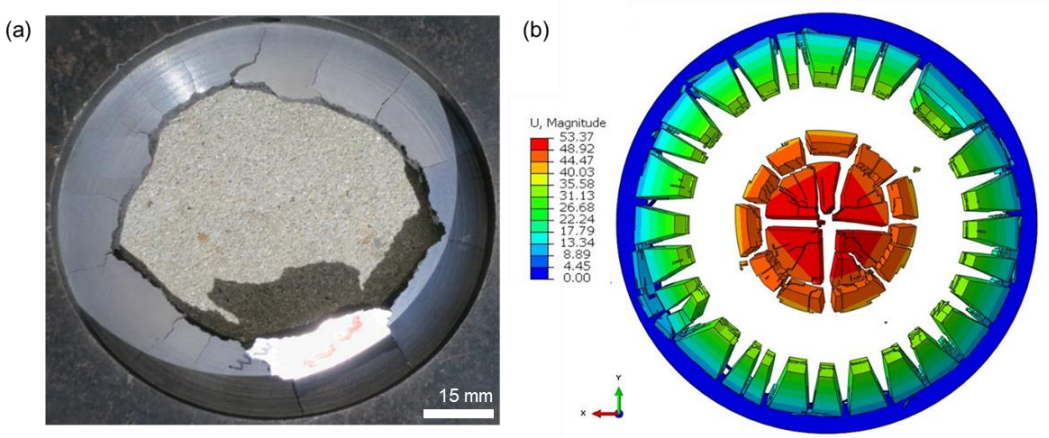

Figure 16. Failure mode of a 3 mm thick syntactic foam subjected to a blast impulse of 2 Ns detonated at a stand-off distance of 180mm (a) Experimental and (b) FEA.

Secondly, the blast response of a thick foam panel (thickness = 14 mm) subjected to an impulse of 4.82 Ns was modelled for validation of the model to capture the related damage profile without the total failure. The simulated failure mode is compared with the experimental one, as shown in Figure 17. The front face shows the damage initiated in the centre with a few cracks propagating radially towards the clamping boundary, as shown in both the experimental and FE results (Fig. 17a). A circumferential crack can also be observed on both the tested and simulated panels where the specimen was clamped. The simulated damage profile on the back face (Fig, 17b) is similar to that on the front face, but with more radial cracks, which captures the experimental failure profile reasonably well. The foam panels tested, with non-homogenous nature, exhibit more random crack patterns in the damaged zones, whereas the homogenous FE models predict damage in a more uniform manner, as expected.

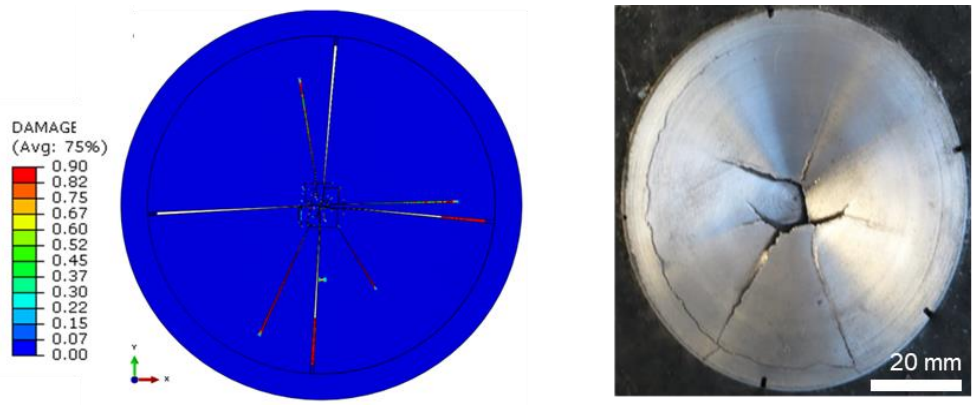

(a) the front face

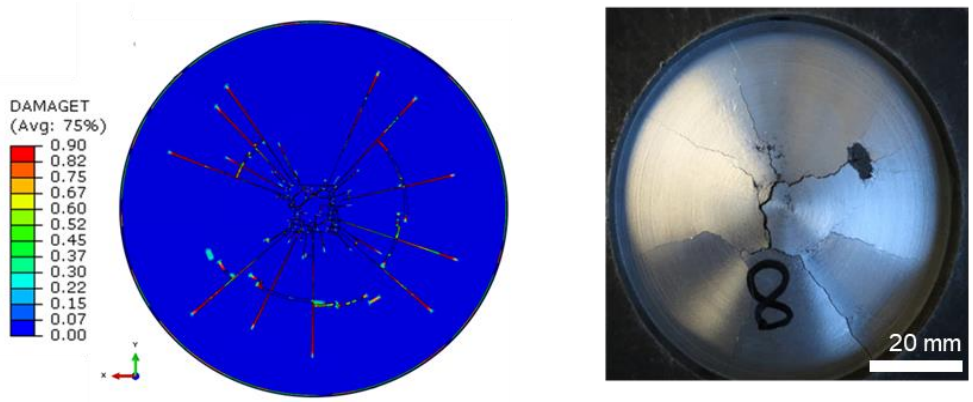

(b) the back face

Figure 17. The predicted and experimental damage profiles of the 14 mm thick syntactic foam subjected to an impulse of 4.82 Ns detonated at a stand-off distance of 180mm.

4.2.4 Prediction of ballistic response of syntactic foams subjected to normal and oblique impacts

The validated FE model was used to study the ballistic impact response of an AK47 projectile impacting on syntactic foams with four different thicknesses. The ballistic limits for these panels were determined to predict the thickness required to stop the projectile for NIJ III standard velocity (750 m/s)[62]. The results for the ballistic limit studies are shown in Figure 18(a), the method of least squares using the Lambert-Jonas equation [61] is used to apply a curve fit to the FE results.

$$V_R = a\left(V_I^b - V_{BL}^b\right)^{\frac{1}{b}} \tag{10}$$

where V_R is the residual velocity, V_I is the impact velocity, V_{BL} is the ballistic limit, a and b are curve fitting constants. From Figure 18(a), it can be seen that in order to achieve a ballistic limit for an impact velocity of 750 m/s (NIJ standard), the required thickness is around 20 mm. The residual velocities for each of the four thicknesses impacted at 750 m/s are shown in Figure 18(b). The simulations of the ballistic impact behaviour using the validated models for normal and oblique impacts are discussed below.

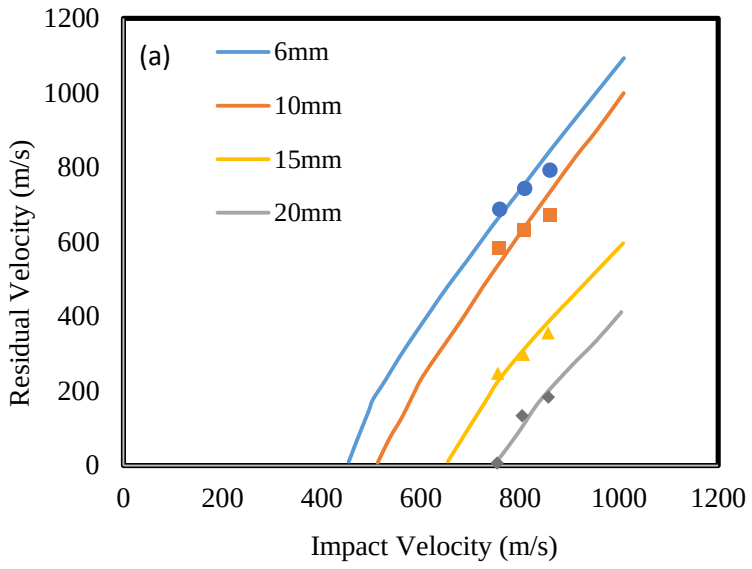

(a)

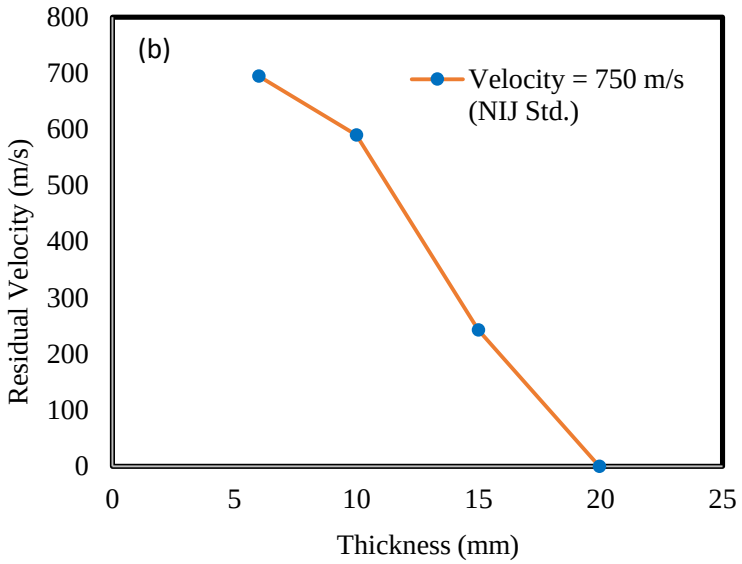

Figure 18. Determining the ballistic limits of different thicknesses (a) $V_R - V_I$ plot for 4 different thicknesses (b) V_R as a function of thickness for V_I = 750 m/s

Normal Impact (90^0)

Most standard ballistic tests are conducted with the projectile impacting perpendicular to the target (normal impact). The FE simulation results for normal impact on the foam panels based on four thicknesses are shown in Figure 19. The contour plots for tensile damage are shown to help study the damage evolution through the various time steps. The 6 mm thick sample (Figures19a-19b) was fully perforated with very little damage to the projectile. The mushrooming of the projectile core can be witnessed for the 10 mm thick sample (Figures 19c-19d). The projectile penetrates the target completely but with a lower residual velocity. Significant deformation of the projectile can be observed during impact on the foam panels with thicknesses of 15 and 20 mm, where the target is able to completely blunt and flatten the projectile front (Figures 19e-19h). The bullet is completely arrested in the 20mm thick sample, even though damage occurs in the back face of the target (Figure 19h). This phenomenon is common in brittle materials, where tensile damage can be seen on the back face even if the projectile is completely stopped. Hence, most armour configurations involving a ceramic front face have a ductile backing material to eliminate damage on the back face.

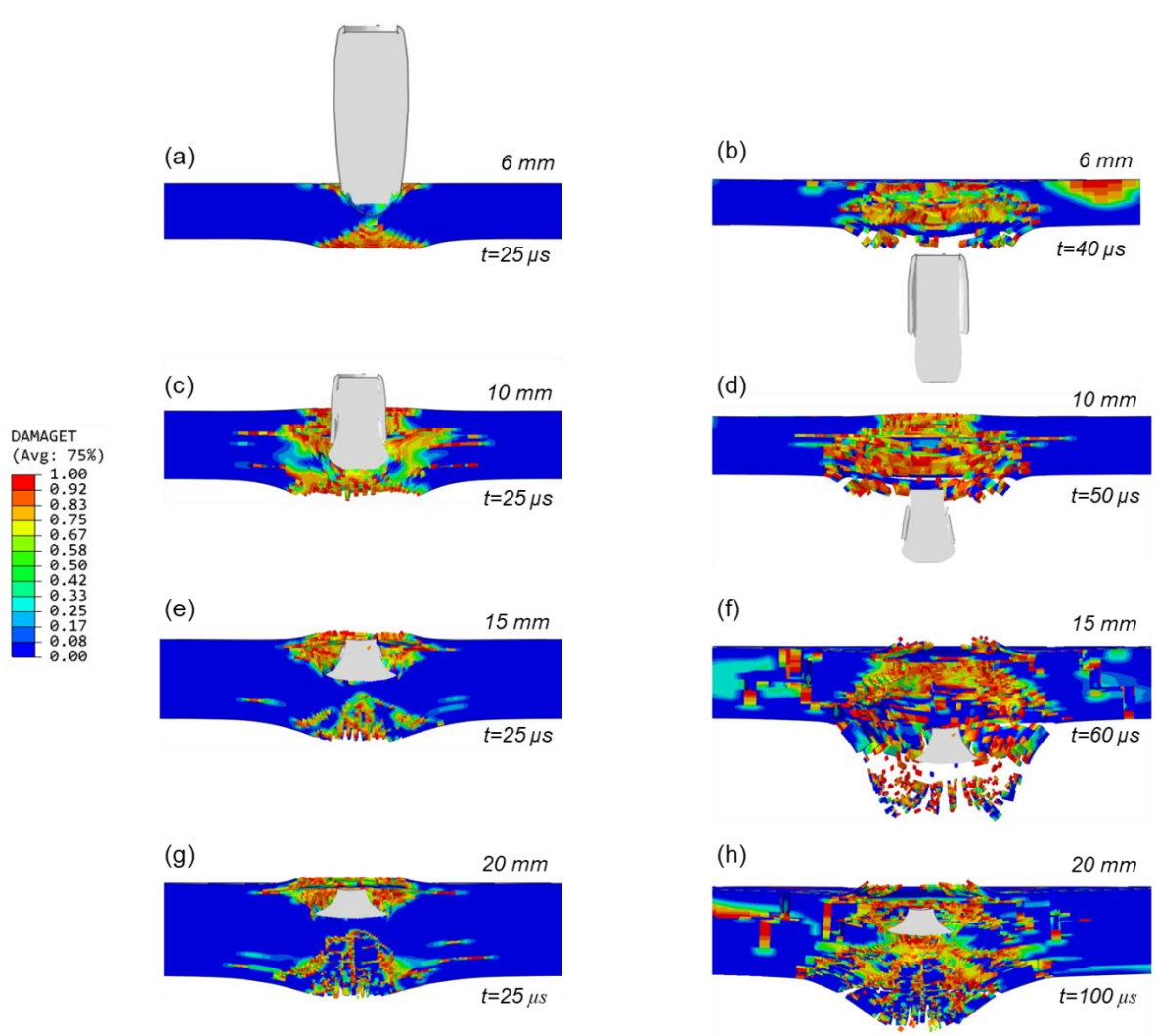

Figure 19. Ballistic simulation results for normal impact (90^0) for 4 different thicknesses shown at 2 different time steps.

Prediction of oblique Impact (30^0 and 45^0)

Ballistic tests performed under normal impact, though critical in determining the ballistic limit, fail to capture the ricochet effect when there are slight variations in the angle of impact. These studies become extremely important when we deal with armour configurations for vehicles and buildings. The FE model setup for oblique impacts at 30° and 45° are shown in Figure 20. The FE simulation results for these oblique impacts are shown in Figures 21 and 22. The 6 mm thick samples are easily perforated in both cases (Figures 21a-21b, Figures 22a-22b), as in the case of normal impact. The angle of impact causes considerable plastic deformation in the projectile and it starts to deform outwards, as can be seen for the foam panels with thicknesses of 10 mm and above. This phenomenon is more evident in 45°

oblique impact cases. The projectile completely perforates the 10 mm target in both cases, while in the 15 mm target, the angle of impact causes the bullet to rotate within the target material (Figure 21f and Figure 22f). The rotated bullet finally bounces back and comes out from the front face of the foam panel. The ricochet effect can be seen in both the 30^0 and 45^0 oblique impacts for a target thickness of 20 mm. The effect is enhanced at higher angles where the bullet slides off the front face resulting in large plastic deformations (Figure 22h).

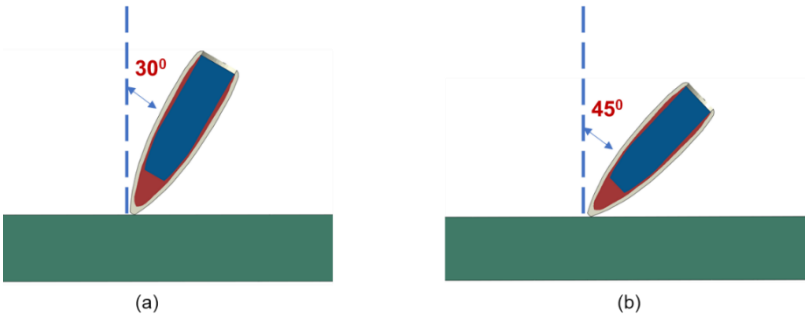

Figure 20. FE model set up for oblique impact (a) 30º impact (b) 45º impact

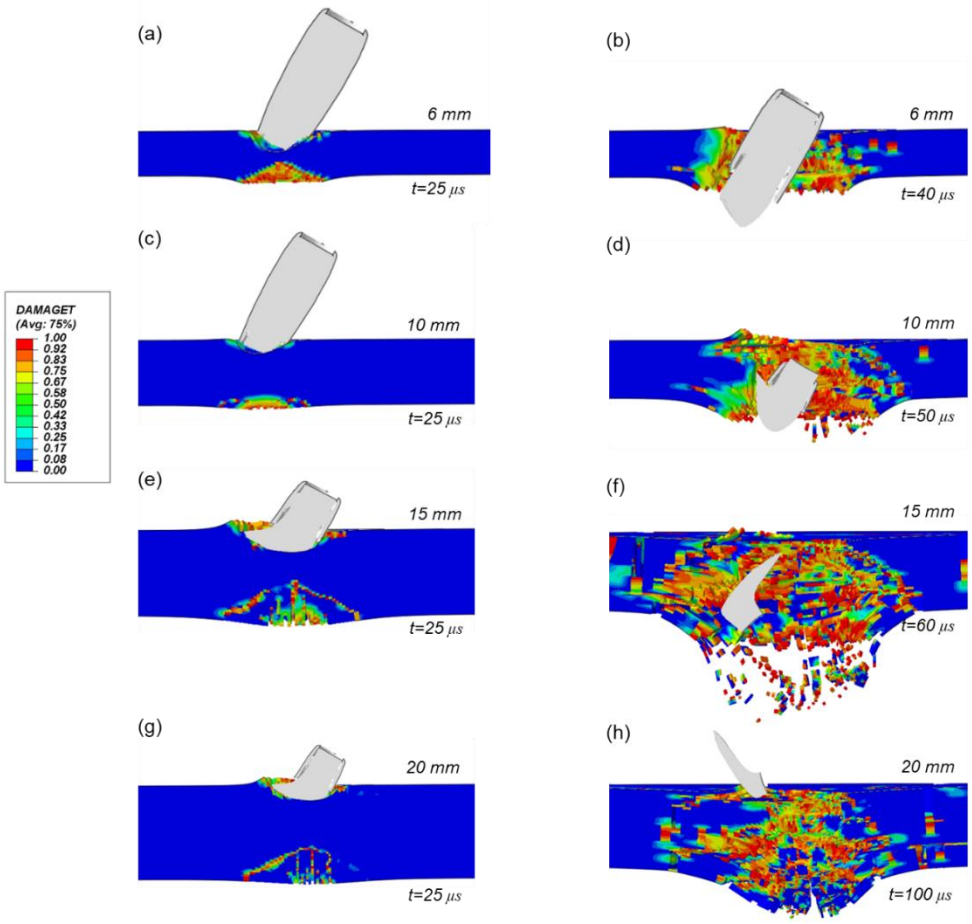

Figure 21. Ballistic simulation results for oblique impact (30º) on 4 different thicknesses of panel at 2 different time steps.

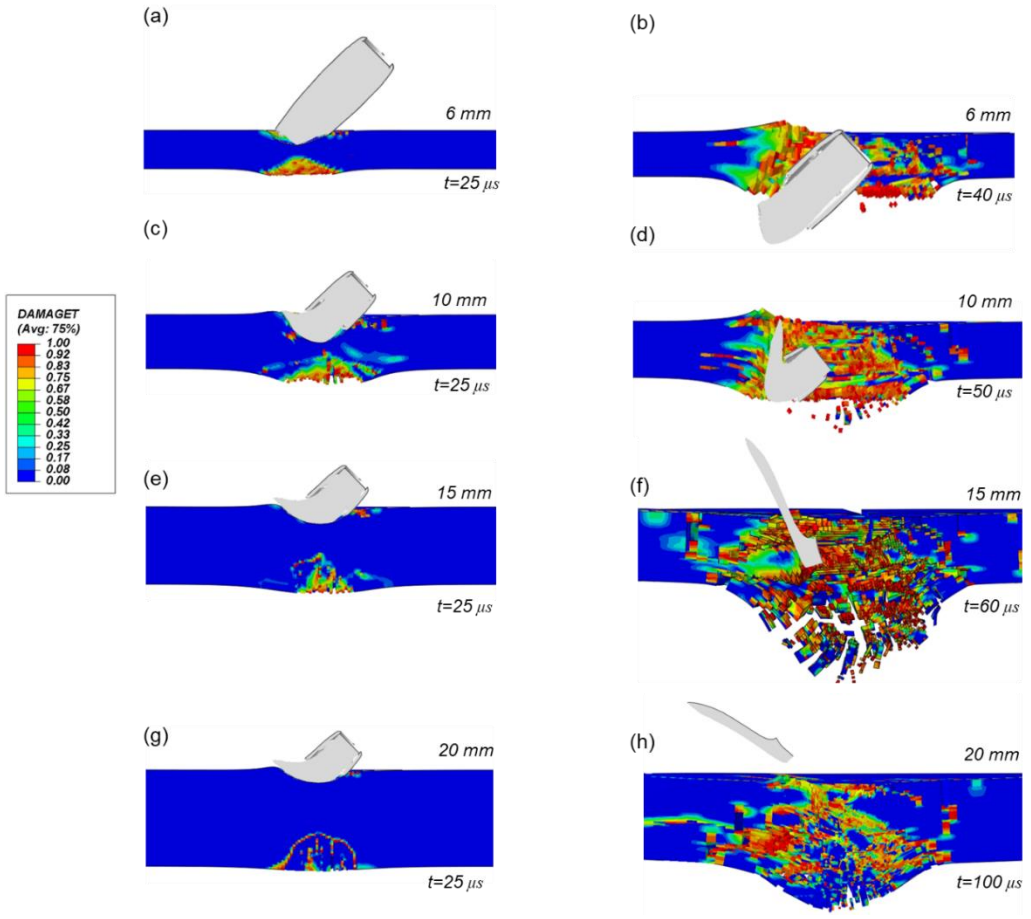

Figure 22. Ballistic simulation results for oblique impact (45º) on 4 different thicknesses of panel at 2 different time steps.

The parametric studies using the validated FE model have provided interesting predictions of impact responses of aluminium matrix syntactic foams subjected to normal and oblique projectile impact, associated with the foams with various thicknesses. The outputs can be used to assisting design of such the foam panels with the homogenised modelling approach.

5. Conclusions

The dynamic response of aluminium matrix syntactic foams subjected to quasi-static and dynamic compression tests, Split Hopkinson Pressure Bar impact, terminal ballistic impact and blast loading have been investigated. Finite element models have been established using Abaqus/Explicit to simulate the dynamic response of the foam under compression, ballistic impact and blast loading. The concrete damaged plasticity model is shown to offer potential for modelling the damage evolution in

such the quasi-brittle materials. The simulations have shown that the FE models capture the essential features of the response of the foams. The ballistic impact model was capable of accurately predicting partial and full perforation of the samples. Parametric studies have been carried out to establish the influence of sample thickness on the ballistic limit velocity. The effect of impact angle on the ballistic performance of these samples has been studied in order to capture ricochet effects. The predictions from the blast model are in a good agreement with the experimental tests. The experimental and modelling studies have led to the following conclusions

(i) Experimental and modelling results for the compression test reveals formation of cracks along a shear plane 45^{o} with the base plane of the specimen consistent with the existing research.

(ii) The SHPB results have shown that the dynamic Young's modulus and the yield strength (peak stress) as well as plateau stress of the aluminium syntactic foams are rate-dependent, with all of them increasing with increasing strain-rate. Such strain-rate sensitivity is even more significant at strain-rates above 1000 s^{-1}.

(iii) The results of ballistic impact tests (normal impact) have shown that 13 mm thick aluminium syntactic foams can stop a projectile at a velocity of 120 m/s. An aluminium syntactic foam with a thickness of 20 mm is required to arrest the 7.62 x 39mm projectile at a standard velocity of 750 m/s. Even though the projectile is arrested within the sample, there is considerable damage at the back face of the specimen, indicating the requirement of a backing material.

(iv) Finite element simulations of oblique impact at a velocity of 750 m/s on syntactic foams show that thicker samples (greater than 10 mm) result in partial or complete rebounding of the projectile, especially at higher impact angles. These studies can be used to identify different strike/back face materials for ensuring the containment of a projectile within the target.

(v) Blast test results have shown that foams with a thickness of 14 mm are able to withstand only low blast loads. The aluminium syntactic foam is too brittle to sustain high blast loads unless it is used as a core material in a sandwich structure.

Acknowledgements

The authors would like to thank Dr Gareth Appleby-Thomas who helps conduct ballistic impact tests in Cranfield University.

References

[1] A.G. Hanssen, L. Enstock, M. Langseth, Close-range blast loading of aluminium foam panels, International Journal of Impact Engineering 27(6) (2002) 593-618.

[2] N. Gupta, P. Rohatgi, Metal matrix syntactic foams : processing, microstructure, properties and applications, 2015.

[3] I.N. Orbulov, K. Májlinger, Description of the compressive response of metal matrix syntactic foams, Materials & Design 49 (2013) 1-9.

[4] L.C. Zou, Q. Zhang, B.J. Pang, G.H. Wu, L.T. Jiang, H. Su, Dynamic compressive behavior of aluminum matrix syntactic foam and its multilayer structure, Materials & Design 45 (2013) 555–560.

[5] L. Licitra, D.D. Luong, O.M. Strbik, N. Gupta, Dynamic properties of alumina hollow particle filled aluminum alloy A356 matrix syntactic foams, Materials & Design 66 (2015) 504-515.

[6] D.K. Balch, D.C. Dunand, Load partitioning in aluminum syntactic foams containing ceramic microspheres, Acta Materialia 54(6) (2006) 1501-1511.

[7] D.K. Balch, J.G. O'Dwyer, G.R. Davis, C.M. Cady, G.T. Gray, D.C. Dunand, Plasticity and damage in aluminum syntactic foams deformed under dynamic and quasi-static conditions, Materials Science and Engineering: A 391(1) (2005) 408-417.

[8] L. Peroni, M. Scapin, M. Avalle, J. Weise, D. Lehmhus, Dynamic mechanical behavior of syntactic iron foams with glass microspheres, Materials Science and Engineering: A 552 (2012) 364-375.

[9] D.D. Luong, V.C. Shunmugasamy, N. Gupta, D. Lehmhus, J. Weise, J. Baumeister, Quasi-static and high strain rates compressive response of iron and Invar matrix syntactic foams, Materials & Design 66 (2015) 516-531.

[10] K. Myers, B. Katona, P. Cortes, I.N. Orbulov, Quasi-static and high strain rate response of aluminum matrix syntactic foams under compression, Composites Part A: Applied Science and Manufacturing 79 (2015) 82-91.

583 [11] D.P. Mondal, S. Das, N. Ramakrishnan, K. Uday Bhasker, Cenosphere filled aluminum syntactic
584 foam made through stir-casting technique, Composites Part A: Applied Science and Manufacturing
585 40(3) (2009) 279-288.
586 [12] M.M. Su, H. Wang, K.Y. Li, H. Hao, Microstructure and Compressive Properties of Al/Al2O3
587 Syntactic Foams, Materials Science Forum 933 (2018) 174-181.
588 [13] C.A. Vogiatzis, A. Tsouknidas, D.T. Kountouras, S. Skolianos, Aluminum–ceramic cenospheres
589 syntactic foams produced by powder metallurgy route, Materials & Design 85 (2015) 444-454.
590 [14] C. San Marchi, F. Cao, M. Kouzeli, A. Mortensen, Quasistatic and dynamic compression of
591 aluminum-oxide particle reinforced pure aluminum, Materials Science and Engineering: A 337(1)
592 (2002) 202-211.
593 [15] J.A. Santa Maria, B.F. Schultz, J.B. Ferguson, P.K. Rohatgi, Al–Al2O3 syntactic foams – Part I:
594 Effect of matrix strength and hollow sphere size on the quasi-static properties of Al-A206/Al2O3
595 syntactic foams, Materials Science and Engineering: A 582 (2013) 415-422.
596 [16] E. Lamanna, N. Gupta, P. Cappa, O.M. Strbik, K. Cho, Evaluation of the dynamic properties of an
597 aluminum syntactic foam core sandwich, Journal of Alloys and Compounds 695 (2017) 2987-2994.
598 [17] Y.M. Chordiya, M.D. Goel, Low Velocity Impact Behavior of Aluminum Cenosphere Syntactic
599 Foam, Materials Today: Proceedings 18 (2019) 3741-3748.
600 [18] Y. Zhang, Y. Zhao, Hysteretic energy dissipation in aluminium matrix syntactic foam under
601 intermittent cyclic compression, Materialia 6 (2019) 100286.
602 [19] I.N. Orbulov, A. Kemény, Á. Filep, Z. Gácsi, Compressive characteristics of bimodal aluminium
603 matrix syntactic foams, Composites Part A: Applied Science and Manufacturing 124 (2019) 105479.
604 [20] I.N. Orbulov, A. Szlancsik, A. Kemény, D. Kincses, Compressive mechanical properties of low-
605 cost, aluminium matrix syntactic foams, Composites Part A: Applied Science and Manufacturing 135
606 (2020) 105923.
607 [21] S. Sahu, M.Z. Ansari, D.P. Mondal, Microstructure and compressive deformation behavior of 2014
608 aluminium cenosphere syntactic foam made through stircasting technique, Materials Today:
609 Proceedings 25 (2020) 785-788.

[22] H. Dave, K. Samvatsar, A comprehensive review on aluminium syntactic foams obtained by dispersion fabrication methods, Materials Today: Proceedings 47 (2021) 4243-4248.

[23] H. Anantharaman, V.C. Shunmugasamy, O.M. Strbik, N. Gupta, K. Cho, Dynamic properties of silicon carbide hollow particle filled magnesium alloy (AZ91D) matrix syntactic foams, International Journal of Impact Engineering 82 (2015) 14-24.

[24] D.P. Mondal, J. Datta Majumder, N. Jha, A. Badkul, S. Das, A. Patel, G. Gupta, Titanium-cenosphere syntactic foam made through powder metallurgy route, Materials & Design 34 (2012) 82-89.

[25] L. Pan, Y. Yang, M.U. Ahsan, D.D. Luong, N. Gupta, A. Kumar, P.K. Rohatgi, Zn-matrix syntactic foams: Effect of heat treatment on microstructure and compressive properties, Materials Science and Engineering: A 731 (2018) 413-422.

[26] A. Daoud, Effect of strain rate on compressive properties of novel Zn12Al based composite foams containing hybrid pores, Materials Science and Engineering: A 525(1) (2009) 7-17.

[27] S. Broxtermann, M. Vesenjak, L. Krstulović-Opara, T. Fiedler, Quasi static and dynamic compression of zinc syntactic foams, Journal of Alloys and Compounds 768 (2018) 962-969.

[28] M.Y. Omar, C. Xiang, N. Gupta, O.M. Strbik, K. Cho, Syntactic foam core metal matrix sandwich composite under bending conditions, Materials & Design 86 (2015) 536-544.

[29] J.B. Ferguson, J.A. Santa Maria, B.F. Schultz, P.K. Rohatgi, Al–Al2O3 syntactic foams—Part II: Predicting mechanical properties of metal matrix syntactic foams reinforced with ceramic spheres, Materials Science and Engineering: A 582 (2013) 423-432.

[30] M.Y. Omar, C. Xiang, N. Gupta, O.M. Strbik, K. Cho, Data characterizing compressive properties of Al/Al2O3 syntactic foam core metal matrix sandwich, Data in Brief 5 (2015) 522-527.

[31] M.Y. Omar, C. Xiang, N. Gupta, O.M. Strbik, K. Cho, Data characterizing flexural properties of Al/Al2O3 syntactic foam core metal matrix sandwich, Data in Brief 5 (2015) 564-571.

[32] D. Luong, O. Strbik, V. Hammond, N. Gupta, K. Cho, Development of high performance lightweight aluminum alloy/SiC hollow sphere syntactic foams and compressive characterization at quasi-static and high strain rates, Journal of Alloys and Compounds 550 (2013) 412-422.

637 [33] M. Su, J. Li, M. Li, H. Hao, Microstructure and mechanical properties of bimodal syntactic foams
638 with different size combination and volume fraction of alumina hollow spheres, Materials Science and
639 Engineering: A 824 (2021) 141798.
640 [34] N. Movahedi, M. Vesenjak, L. Krstulović-Opara, I.V. Belova, G.E. Murch, T. Fiedler, Dynamic
641 compression of functionally-graded metal syntactic foams, Composite Structures 261 (2021) 113308.
642 [35] M. Salehi, S.M.H. Mirbagheri, A.J. Ramiani, Efficient energy absorption of functionally-graded
643 metallic foam-filled tubes under impact loading, Transactions of Nonferrous Metals Society of China
644 31(1) (2021) 92-110.
645 [36] M. Bhandari, K. Purohit, Dynamic Fracture Analysis of Functionally Graded Material Structures –
646 A Critical Review, Composites Part C: Open Access 7 (2022) 100227.
647 [37] I.N. Orbulov, Metal matrix syntactic foams produced by pressure infiltration—The effect of
648 infiltration parameters, Materials Science and Engineering: A 583 (2013) 11-19.
649 [38] A. S-de-la-Muela, L. Cambronero, J. Ruiz Román, Molten Metal Infiltration Methods to Process
650 Metal Matrix Syntactic Foams, Metals 10 (2020) 149.
651 [39] X.F. Tao, Y.Y. Zhao, Compressive behavior of Al matrix syntactic foams toughened with Al
652 particles, Scripta Materialia 61(5) (2009) 461-464.
653 [40] M.D. Goel, M. Peroni, G. Solomos, D.P. Mondal, V.A. Matsagar, A.K. Gupta, M. Larcher, S.
654 Marburg, Dynamic compression behavior of cenosphere aluminum alloy syntactic foam, Materials &
655 Design 42 (2012) 418-423.
656 [41] M. Altenaiji, Z.W. Guan, W.J. Cantwell, Y. Zhao, G.K. Schleyer, Characterisation of aluminium
657 matrix syntactic foams under drop weight impact, Materials & Design 59 (2014) 296-302.
658 [42] V.S. Deshpande, N.A. Fleck, High strain rate compressive behaviour of aluminium alloy foams,
659 International Journal of Impact Engineering 24(3) (2000) 277-298.
660 [43] K. Dharmasena, H.N.G. Wadley, Z. Xue, J. Hutchinson, Mechanical Response of Metallic
661 Honeycomb Sandwich Panel Structures to High-Intensity Dynamic Loading, International Journal of
662 Impact Engineering - INT J IMPACT ENG 35 (2008) 1063-1074.
663 [44] Z. Fan, F. Zhang, B. Zhang, T. He, P. Xu, X. Cai, Modelling the dynamic compressive response of
664 syntactic foam with hierarchical cell structure, Cement and Concrete Composites 124 (2021) 104248.

[45] Y. Wang, Q. Liu, B. Zhang, H. Zhang, Y. Jin, Z. Zhong, J. Ye, Y. Ren, F. Ye, W. Wang, Dynamic compressive response and impact resistance of bioinspired nacre-like 2024Al/B4C composites, Materials Science and Engineering: A 831 (2022) 142261.

[46] Z. Li, Z. Zheng, J. Yu, Low-velocity perforation behavior of composite sandwich panels with aluminum foam core, Journal of Sandwich Structures and Materials 15 (2012) 92-109.

[47] D. Radford, G. McShane, V.S. Deshpande, N. Fleck, The response of clamped sandwich plates with metallic foam cores to simulated blast loading, International Journal of Solids and Structures - INT J SOLIDS STRUCT 43 (2006) 2243-2259.

[48] H. Kolsky, An Investigation of Mechanical Properties of Materials at Very High Rates of Loading, Proceedings of the Physical Society. Section B 62 (2002) 676.

[49] I.G. Crouch, G. Appleby-Thomas, P.J. Hazell, A study of the penetration behaviour of mild-steel-cored ammunition against boron carbide ceramic armours, International Journal of Impact Engineering 80 (2015) 203-211.

[50] N. Jacob, S. Chung Kim Yuen, G.N. Nurick, D. Bonorchis, S.A. Desai, D. Tait, Scaling aspects of quadrangular plates subjected to localised blast loads—experiments and predictions, International Journal of Impact Engineering 30(8) (2004) 1179-1208.

[51] R. Wharton, S.A. Formby, R. Merrifield, Airblast TNT equivalence for a range of commercial blasting explosives, Journal of hazardous materials 79 (2001) 31-9.

[52] G. Nurick, G. Langdon, Y. Chi, N. Jacob, Behaviour of sandwich panels subjected to intense air blast – Part 1: Experiments, Composite Structures - COMPOS STRUCT 91 (2009) 433-441.

[53] M. Yahya, The Blast Response of Fibre Reinforced Composites and Sandwich Structures, University of Liverpool, 2008.

[54] Abaqus, Abaqus documentation, Version 6 (2014) 1-5.

[55] G.R. Johnson, W.H. Cook, Fracture characteristics of three metals subjected to various strains, strain rates, temperatures and pressures, Engineering Fracture Mechanics 21(1) (1985) 31-48.

[56] L. Carbajal, J. Jovicic, H. Kuhlmann, Assault Riffle Bullet-Experimental Characterization and Computer (FE) Modeling, Conference proceedings of the Society for Experimental Mechanics Series. Experimental and applied mechanics 6 (2011).

693 [57] Z.W. Guan, A. Aktas, P. Potluri, W.J. Cantwell, G. Langdon, G.N. Nurick, The blast resistance of
694 stitched sandwich panels, International Journal of Impact Engineering 65 (2014) 137-145.
695 [58] R.G. Teeling-Smith, G.N. Nurick, The deformation and tearing of thin circular plates subjected to
696 impulsive loads, International Journal of Impact Engineering 11(1) (1991) 77-91.
697 [59] I. Kozma, D. Harangozó, H. Hargitai, I. Zsoldos, DISPLACEMENT-BASED FAILURE
698 ANALYSIS OF METAL MATRIX SYNTACTIC FOAM, 2019.
699 [60] I. Kozma, I. Zsoldos, CT-based tests and finite element simulation for failure analysis of syntactic
700 foams, Engineering Failure Analysis 104 (2019) 371-378.
701 [61] G.H. Jonas, J.A. Zukas, Mechanics of penetration: Analysis and experiment, International Journal
702 of Engineering Science 16(11) (1978) 879-903.
703 [62] A. Bhatnagar, 5 - Standards and specifications for lightweight ballistic materials, in: A. Bhatnagar
704 (Ed.), Lightweight Ballistic Composites, Woodhead Publishing2006, pp. 127-167.

705